HHS Public Access

Author manuscript

J Pharmacokinet Pharmacodyn. Author manuscript; available in PMC 2016 October 01.

Published in final edited form as:

J Pharmacokinet Pharmacodyn. 2015 October ; 42(5): 541–552. doi:10.1007/s10928-015-9445-x.

Physiologically-based Pharmacokinetic Modeling of Target-Mediated Drug Disposition of Bortezomib in Mice

Li Zhang and **Donald E. Mager**

Department of Pharmaceutical Sciences, University at Buffalo, State University of New York, Buffalo, New York

Abstract

Bortezomib is a reversible proteasome inhibitor with potent antineoplastic activity that exhibits dose- and time-dependent pharmacokinetics (PK). Proteasome-mediated bortezomib disposition is proposed as the primary source of its nonlinear and apparent nonstationary PK behavior. Single intravenous (IV) doses of bortezomib (0.25 and 1 mg/kg) were administrated to BALB/c mice, with blood and tissue samples obtained over 144 hours, which were analyzed by LC/MS/MS. A physiologically based pharmacokinetic (PBPK) model incorporating tissue drug-target binding was developed to test the hypothesis of proteasome-mediated bortezomib disposition. The final model reasonably captured bortezomib plasma and tissue PK profiles, and parameters were estimated with good precision. The rank-order of model estimated tissue target density correlated well with experimentally measured proteasome concentrations reported in the literature, supporting the hypothesis that binding to proteasome influences bortezomib disposition. The PBPK model was further scaled-up to humans to assess the similarity of bortezomib disposition among species. Human plasma bortezomib PK profiles following multiple IV dosing (1.3 mg/m^2) on days 1, 4, 8, and 11 were simulated by appropriately scaling estimated mouse parameters. Simulated and observed bortezomib concentrations after multiple dosing were in good agreement, suggesting target-mediated bortezomib disposition is likely for both mice and humans. Furthermore, the model predicts that renal impairment should exert minimal influence on bortezomib exposure in humans, confirming that bortezomib dose adjustment is not necessary for patients with renal impairment.

Keywords

bortezomib; physiologically-based pharmacokinetics; proteasome binding; target-mediated drug disposition

INTRODUCTION

Bortezomib (Velcade®), a reversible proteasome inhibitor, shows potent antineoplastic activity by inhibiting the constitutively elevated proteasome activity in myeloma cells and is approved as a first-line therapy for patients with multiple myeloma (MM) [1]. Apart from its

Corresponding Author: Dr. Donald E. Mager, Department of Pharmaceutical Sciences, University at Buffalo, State University of New York, Buffalo, NY, 14214, Tel: (716) 645-2903, Fax: (716) 829-6569, dmager@buffalo.edu.

potent anti-myeloma effects, bortezomib is also being evaluated for the treatment of solid tumors, such as lung and breast cancers [2]. Despite these salutary effects, dose-limiting toxicities, such as thrombocytopenia, anemia and diarrhea, still pose challenges to its clinical utilization [3, 4], and more research into bortezomib concentration-effect relationships is needed to identify sources of individual variability in clinical outcomes. The pharmacokinetics (PK) of bortezomib is characterized by dose- and time-dependent disposition properties, which might influence its tissue selectivity and resulting systemic adverse effects [5]. However, the determinants of this nonlinear behavior have not been well delineated, and exploring the source(s) of bortezomib nonlinear and nonstationary PK may provide insights into improving its clinical use.

Bortezomib plasma PK profiles after intravenous (IV) injection show a steep distributive phase, which becomes saturated at higher dose levels, followed by a long terminal elimination phase. Bortezomib moderately binds to plasma proteins (approximately 83%), with linear binding properties reported at therapeutic concentrations [5]. Hepatic and renal clearance are the major elimination pathways, and bortezomib undergoes linear liver metabolism at clinically relevant concentrations [6]. However, the contribution of hepatic clearance to overall bortezomib elimination remains unknown in mice and humans [7]. With regards to drug distribution, a preclinical study suggests that bortezomib rapidly and extensively distributes into tissues, including the bone marrow (target tissue) and tissues associated with adverse effects (e.g., erythrocytes and liver). High concentrations of bortezomib in erythrocytes are mainly attributed to its extensive binding to cytosolic proteasome [8]. Moreover, bortezomib erythrocyte distribution is concentration-dependent owing to saturable drug-proteasome binding [9]. Since proteasome is a highly conserved protease complex in the cytoplasm and expressed in all tissues with various densities [2, 10, 11], we hypothesize that saturable binding of bortezomib to proteasome is the primary source for its nonlinear PK behavior.

Dr. Gerhard Levy was the first to coin the name target-mediated drug disposition (TMDD) for describing the unique PK characteristics of such compounds, in which the interaction with high-affinity low-capacity targets significantly influences drug kinetics [12]. His initial focus was on small molecular weight compounds, such as warfarin, that displayed concentration- and time-dependent changes in tissue distribution [12, 13]. Over the subsequent two decades, appreciation of TMDD has substantially increased, primarily due to its role in the PK of many peptides, proteins, and antibody-based therapeutics [14]. Interestingly, there has been a resurgence in the development of covalent drugs [15], and several of these small molecular weight compounds are known or suspected to exhibit TMDD. A general compartmental modeling framework has been developed [16], and applications of this full modeling approach, along with several approximations [17], have shown considerable utility in characterizing complex TMDD profiles and features [18]. In contrast to compartmental modeling, physiologically-based PK (PBPK) models can be particularly informative in assessing the influence of tissue target binding on the disposition processes of drugs [19]. Levy and colleagues developed an integrated PBPK model for warfarin, by incorporating experimentally determined target density and affinity values in tissues, which well recapitulated the resultant concentration- and time-dependent warfarin biodistribution in rats [20]. Despite extensive clinical experience with bortezomib, no

mathematical modeling for investigating bortezomib PK has been published. This study aims to develop a PBPK model to investigate the influence of saturable tissue drug-target binding on bortezomib disposition in mice. The PBPK model was further scaled-up to test our hypothesis of target-mediated bortezomib disposition in humans. In addition, the renal component of the model was used to theoretically assess the influence of renal dysfunction on bortezomib exposure in humans.

MATERIALS AND METHODS

Chemicals

Bortezomib (Velcade®) was purchased from Millennium Pharmaceuticals Inc. (Cambridge, MA, USA). Assay standard bortezomib, the quality control in LC/MS/MS analysis, was purchased from LC laboratories (Woburn, MA, USA) with chemical purities greater than 99%. The internal standard (IS), bortezomib-deuterium8 (bortezomib-d8), was purchased from Toronto Research Chemicals (Toronto, Canada). HPLC-grade methanol, acetonitrile, and water were obtained from J.T Baker (Phillipsburg, NJ, USA). Formic acid, phosphoric acid, and acetic acid were purchased from Sigma-Aldrich (St Louis, MO). Blank mouse plasma was obtained from Lampire Biological Laboratories (Pipersville, PA, USA).

Bortezomib PK study in BALB/c mice

Male BALB/c mice weighing 22–28 grams (4–5 week old) were purchased from Harlan (Indianapolis, IN). Mice were housed in a temperature-controlled environment on a standard light-dark cycle and with free access to standard diet and water. This animal study was approved by the Institutional Animal Care and Use Committee, at the University at Buffalo, SUNY.

Mice were randomly divided into two groups according to body weight, and a single intravenous (IV) bolus dose of bortezomib (0.25 or 1 mg/kg) was administered to mice via penile vein injection. Three mice in each group were sacrificed for terminal sampling of blood, liver, kidney, spleen, lung, muscle, and bone at each time point: 10 min, and 1, 3, 8, 24, 72, 120 and 144 hr following drug administration. Additional blood samples were also collected at 3 min after bortezomib injection. Plasma was obtained from blood by centrifugation at 3000 rpm for 10 min at 4 °C. 2% formic acid was spiked into plasma and whole blood to prevent drug degradation. Entire organs of liver, kidney, spleen and lung (along with representative samples of skeletal muscle and bone) were collected for drug quantification. All samples were stored at −80 °C until further analysis.

Bortezomib LC/MS/MS Analysis

A sensitive LC/MS/MS method was established to analyze bortezomib concentrations in mouse plasma and tissue samples. Tissue samples were prepared by homogenization in a fixed volume of 20% acetonitrile with 2% formic acid on ice to avoid degradation. Briefly, 10 μL of bortezomib standard and bortezomib-d8 (IS) were spiked in 50 μL of mouse plasma or tissue homogenate, and protein was precipitated using phosphoric acid followed by centrifugation. 350 μL of supernatant was taken for solid phase extraction (SPE) on Oasis® HLB cartridges (Waters Corp., Milford, MA), with cartridges subsequently washed

with 2% phosphoric acid and 30% methanol. Analytes were eluted by methanol with 0.1% acetic acid. Elutes were evaporated and reconstituted in 250 μL of 20% acetonitrile for LC/MS/MS injection. LC/MS/MS was performed on a Shimazu HPLC system coupled to an API-3000 triple-quadrupole mass spectrometer. Chromatographic separation was conducted on a Waters Xbridge C8 column (2.1 × 50 mm, 3.5 μm). A binary gradient mobile phase of (A) 5% acetonitrile with 0.1% formic acid and (B) 95% acetonitrile with 0.1% formic acid was used for analyte elution. Analyte and IS were detected in MRM mode of positive ESI. Monitored transitions were 367.2 > 226.2 for bortezomib and 375.3 > 234.2 for bortezomib-d8. Excellent linearity was obtained for the calibration curve over the concentration range of 1.3 – 2603 nM (r = 0.9997), and the limit of quantification (LOQ) was 1.3 nM in plasma and 2.6 nM in tissue homogenate. Good inter-day and intra-day precision with RSD% <10%, as well as accuracy with bias < 10%, were obtained for bortezomib in plasma and tissue samples.

Bortezomib PBPK Model Development

Construction of the bortezomib PBPK model was performed in several stages. Firstly, the linearity of bortezomib PK was assessed by non-compartmental analysis (NCA) of plasma and tissue concentration data. The area under drug concentration curve (AUC), partition coefficient (K_P, defined as the ratio of tissue-to-plasma AUC), and terminal half-life for each tissue were calculated using the linear trapezoidal rule (Table 1). Secondly, local models were developed and fitted to each tissue individually, and estimated parameters obtained from local model fitting were then used as initial estimates for developing the global PBPK model. As bortezomib is eliminated primarily through hepatic and renal clearance [5], the liver and kidney compartments were considered as eliminating organs in model. During model development, physiological system-specific parameter values, such as tissue volumes, blood flows, tissue vascular fractions, hematocrit (HCT = 0.45), and GFR, were fixed to literature reported values, along with known bortezomib-specific parameters, such as proteasome binding affinity (K_D = 0.6 nM) and plasma protein unbound fraction (f_u = 0.17) (Table 2) [5, 21–23].

Local model fitting

Bortezomib plasma PK profiles were characterized by an explicit tri-exponential function, and then each tissue was fitted individually using a hybrid-PBPK approach, in which plasma PK was fixed as the kinetic driving force. Blood was divided into plasma and red blood cells (RBC), wherein nonlinear target binding occurs (Fig. 1). Drug exchange between plasma and RBC was described in terms of permeability-surface area coefficient PS_{bc} and a nonlinear partition coefficient P_{bc}. Furthermore, each tissue compartment was comprised of i) a tissue extravascular space, and ii) a tissue vascular compartment that was further subdivided into tissue plasma and tissue RBC spaces. Nonlinear drug-target binding was proposed to occur in both tissue blood cells as well as tissue extravascular space with the same target binding affinity K_D. Drug exchange between tissue plasma and tissue extravascular compartments was defined in terms of permeability-limited distribution (PS_{ti}) as well as nonlinear partitioning ($P_{tc,ti}$).

Global PBPK model

The optimized local models for various tissues were linked by a plasma and RBC flow network to build a whole-body bortezomib PBPK model (Fig. 2), in which all non-assayed tissues (e.g., gastrointestinal and adipose) were lumped into a remainder compartment. Hepatic clearance was proposed to occur in the tissue extravascular compartment, and renal clearance occurs from the plasma space in the kidney compartment. The following differential equations were used to describe bortezomib disposition in mice:

Blood (*bl*):

$$[V_{bl}\cdot(1-HCT)]\cdot\frac{dC_p}{dt}=Q_p\cdot(C_{p,lu}-C_p)-PS_{bc}\cdot(C_p-\frac{C_{bc}}{P_{bc}}) \quad (1)$$

$$(V_{bl}\cdot HCT)\cdot\frac{dC_{bc}}{dt}=Q_{bc}\cdot(C_{bc,lu}-C_{bc})+PS_{bc}\cdot(C_p-\frac{C_{bc}}{P_{bc}}) \quad P_{bc}=NS_{bc}+\frac{R_{\max}}{K_D+C_p} \quad (2)$$

Non-eliminating tissues (*ti*):

$$V_{p,ti}\cdot\frac{dC_{p,ti}}{dt}=Q_{p,ti}\cdot(C_p-C_{p,ti})-PS_{bc}\cdot(C_{p,ti}-\frac{C_{bc,ti}}{P_{bc,ti}})-PS_{tc,ti}\cdot(C_{p,ti}-\frac{C_{tc,ti}}{P_{tc,ti}}) \quad (3)$$

$$V_{bc,ti}\cdot\frac{dC_{bc,ti}}{dt}=Q_{bc,ti}\cdot(C_{bc}-C_{bc,ti})+PS_{bc}\cdot(C_{p,ti}-\frac{C_{bc,ti}}{P_{bc,ti}}) \quad (4)$$

$$V_{tc,ti}\cdot\frac{dC_{tc,ti}}{dt}=PS_{tc,ti}\cdot(C_{p,ti}-\frac{C_{tc,ti}}{P_{tc,ti}}) \quad (5)$$

Liver (*li*):

$$V_{p,li}\cdot\frac{dC_{p,li}}{dt}=Q_{p,sp}\cdot C_{p,sp}+(Q_{p,li}-Q_{p,sp})\cdot(C_p-C_{p,li})-PS_{bc}\cdot(C_{p,li}-\frac{C_{bc,li}}{P_{bc,li}})-PS_{tc,li}\cdot(C_{p,li}-\frac{C_{tc,li}}{P_{tc,li}}) \quad (6)$$

$$V_{bc,li}\cdot\frac{dC_{bc,li}}{dt}=Q_{bc,sp}\cdot C_{bc,sp}+(Q_{bc,li}-Q_{bc,sp})\cdot(C_{bc}-C_{bc,li})+PS_{bc}\cdot(C_{p,li}-\frac{C_{bc,li}}{P_{bc,li}}) \quad (7)$$

$$V_{tc,li}\cdot\frac{dC_{tc,li}}{dt}=PS_{tc,li}\cdot(C_{p,ti}-\frac{C_{tc,li}}{P_{tc,li}})-CL_{\text{int}}\cdot C_{tc,li} \quad (8)$$

Kidney (*ki*):

$$V_{p,ki}\cdot\frac{dC_{p,ki}}{dt}=Q_{p,ki}\cdot(C_p-C_{p,ki})-PS_{bc}\cdot(C_{p,ki}-\frac{C_{bc,ki}}{P_{bc,ki}})-PS_{tc,ki}\cdot(C_{p,ki}-\frac{C_{tc,ki}}{P_{tc,ki}})-CL_r\cdot f_u\cdot C_{p,ki} \quad CL_r=GFR \quad (9)$$

$$V_{bc,ki} \cdot \frac{dC_{bc,ki}}{dt} = Q_{bc,ki} \cdot (C_{bc} - C_{bc,ki}) + PS_{bc} \cdot (C_{p,ki} - \frac{C_{bc,ki}}{P_{bc,ki}}) \quad (10)$$

$$V_{tc,ki} \cdot \frac{dC_{tc,ki}}{dt} = PS_{tc,ki} \cdot (C_{p,ki} - \frac{C_{tc,ki}}{P_{tc,ki}}) \quad (11)$$

Lung (*lu*):

$$V_{p,lu} \cdot \frac{dC_{p,lu}}{dt} = (\sum Q_{p,ti} \cdot C_{p,ti} - Q_{lu,ti} \cdot C_{p,lu}) - PS_{bc} \cdot (C_{p,lu} - \frac{C_{bc,lu}}{P_{bc,lu}}) - PS_{tc,lu} \cdot (C_{p,lu} - \frac{C_{tc,lu}}{P_{tc,lu}}) \quad (12)$$

$$V_{bc,lu} \cdot \frac{dC_{bc,lu}}{dt} = (\sum Q_{bc,ti} \cdot C_{bc,ti} - Q_{bc,ti} \cdot C_{bc,lu}) + PS_{bc} \cdot (C_{p,lu} - \frac{C_{bc,lu}}{P_{bc,lu}}) \quad (13)$$

$$V_{tc,lu} \cdot \frac{dC_{tc,lu}}{dt} = PS_{tc,lu} \cdot (C_{p,lu} - \frac{C_{tc,lu}}{P_{tc,lu}}) \quad (14)$$

Tissue subcompartment volumes:

$$V_{p,ti} = V_{ti} \cdot fv_{,ti} \cdot (1 - HCT) \quad (15)$$

$$V_{bc,ti} = V_{ti} \cdot fv_{,ti} \cdot HCT \quad (16)$$

$$V_{tc,ti} = V_{ti} \cdot (1 - fv_{,ti}) \quad (17)$$

with symbols representing plasma flow (Q_p), RBC flow(Q_{bc}), tissue plasma flow ($Q_{p,ti}$), blood volume (V_{bl}), tissue RBC flow ($Q_{bc,ti}$), tissue vascular fraction ($fv_{,ti}$), tissue volume (V_{ti}), tissue plasma volume ($V_{p,ti}$), tissue RBC volume ($V_{bc,ti}$), tissue extravascular volume ($V_{tc,ti}$), hepatic intrinsic clearance (CL_{int}), and renal clearance (CL_r). $C_{p,ti}$, $C_{bc,ti}$, and $C_{tc,ti}$ represent drug concentrations in tissue plasma, tissue erythrocytes, and tissue cellular spaces. P_{bc} is the nonlinear partition ratio of bortezomib in RBC. The tissue RBC-to-plasma nonlinear partition ratio ($P_{bc,ti}$), as well as the tissue extravascular-to-plasma partition ratio ($P_{tc,ti}$), were defined as:

$$P_{bc,ti} = NS_{bc} + \frac{R_{\max}}{K_D + C_{p,ti}} \quad (18)$$

$$P_{tc,ti} = NS_{ti} + \frac{R_{ti}}{K_D + C_{p,ti}} \quad (19)$$

with R_{max} and R_{ti} representing target capacity in RBC and tissue extravascular spaces. NS_{bc} and NS_{ti} are used to accommodate nonspecific binding of bortezomib in RBC as well as in tissue extravascular spaces. The initial conditions for Eqs. 1–14 were set to zero.

Interspecies scaling

The global PBPK model developed for mice was scaled-up for humans to assess the ability of the target-mediated PBPK structure to describe bortezomib disposition in humans. Physiological values of tissue volume, blood flow, tissue vascular fraction, *HCT*, *GFR*, and f_u were fixed to human literature values [5, 21]. Proteasome density, target binding affinity, and nonspecific binding in humans were assumed to be identical with those in mice. Human hepatic clearance ($CL_{int,h}$) and the permeability-limited distribution coefficient ($PS_{ti,h}$) were predicted from values estimated in mice using allometric scaling:

$$P_{,h}=P_{,mice}\cdot\left(\frac{BW_{,h}}{BW_{,mice}}\right)^{B} \quad (20)$$

With $P_{,h}$ as the human parameter of interest and *BW* is species body weight. *B* is an allometric exponent, which was fixed to 0.75 for $CL_{int,h}$ scaling. In addition, the permeability of tissue cellular membranes, as well as organ structure, was assumed to be geometrically similar among mammals. Therefore, the value of *B* was fixed at 0.67 for human PS_{bc} and $PS_{tc,ti}$ extrapolations [24]. The final PK parameters used to simulate human PK are provided in Supplementary Table S1.

Data analysis

Parameter estimates were obtained by model fitting to plasma and tissue data simultaneously using the maximum likelihood algorithm in ADAPT5 [25]. The variance model was defined as:

$$V_i=(\sigma_1+\sigma_2\cdot Y_i)^2 \quad (21)$$

with σ_1 and σ_2 as the estimated variance model parameters, and Y_i represents model predicted values. Model selection was based on goodness-of-fit criteria, which included Akaike information criterion, estimation criterion value, confidence intervals of parameter estimates, and visual inspection of predicted versus observed and residual plots.

RESULTS

Bortezomib PK in mice

Bortezomib PK profiles following single IV dosing of 0.25 and 1 mg/kg in mice are shown in Figure 3. Bortezomib plasma and tissue PK profiles exhibit steep distribution phases followed by long terminal elimination phases. The concentrations in tissues are one- to two-orders of magnitude greater than plasma concentrations over the entire PK profile, indicating bortezomib has extensive tissue distribution. Notably, the terminal phases of non-eliminating tissues start to converge toward similar concentrations at different dose levels. In addition, NCA analysis results indicate a disproportional change in K_p with increasing dose

for each non-eliminating tissue, indicating nonlinear tissue partitioning (Table 1). Moreover, bortezomib PK exhibited properties of high- affinity but low-capacity target binding in tissues, where the tissue-to-plasma concentration ratios of non-eliminating tissues all exhibited high values at low plasma concentration, and the ratio decreased when plasma concentrations were high after the 0.25 mg/kg dose level (data not shown). These PK characteristics, together with other research findings [8, 9], suggest the highly specific, but capacity-limited, drug-proteasome binding played an important role in nonlinear PK behavior of bortezomib. Accordingly, saturable tissue target binding was proposed to describe bortezomib nonlinear tissue partitioning.

Bortezomib global PBPK Model

A whole-body PBPK model (Fig. 2) was developed by incorporating saturable target binding to capture nonlinear bortezomib tissue distribution, which was connected by plasma and RBC circulation as the inter-tissue transfer flow. The PBPK model simultaneously captured bortezomib PK profiles in plasma and tissues reasonably well (Fig. 3), and the final model parameters were estimated with good precision (low CV%) (Table 3). Initial attempts of estimating permeability coefficients for erythrocytes using the global PBPK model resulted in unidentifiable parameter estimates and were therefore fixed to the estimate from local model fitting. Michaelis-Menten kinetics was first tried to characterize hepatic clearance; however, the clearance K_m value could not be identified (i.e., estimated with high CV%). Based on the poor estimation of such parameters and literature reports of linear hepatic metabolism [6], bortezomib hepatic clearance was proposed to be described by a linear function in the final PBPK model. Apart from erythrocytes, the estimated values of permeability coefficients ($PS_{tc.ti}$) were lower than corresponding tissue blood flow, warranting the permeability-limited distribution model for capturing tissue kinetics. The fitted proteasome density in the remainder compartment was relatively high, which could be attributed to the non-sampled tissues with high proteasome density, such as *mesenteric lymph node* and intestine, being lumped into the remainder space [11, 26]. In addition, the rank-order of tissue target density estimated by model fitting correlated well with experimentally reported proteasome concentrations in rat tissues (Fig. 4a) [9, 11], supporting the hypothesis of target-mediated bortezomib disposition. The rank-order of bortezomib tissue exposure correlated with tissue target density, suggesting tissue proteasome density is a crucial factor determining the selectivity and extent of bortezomib tissue distribution (Fig. 4b). Moreover, the PBPK model was further validated by recapitulating bortezomib blood PK following 0.8 mg/kg IV dosing in mice, and the good agreement between simulated and experimental data added confidence in the final PBPK model (Supplementary Fig. S1).

Interspecies scaling to human

To further assess the similarity of bortezomib disposition among different species, the ability of the PBPK model to predict bortezomib PK in humans was evaluated. Human plasma PK profiles following multiple IV dosing of bortezomib (1.3 mg/m^2) on day 1, 4, 8, and 11 were simulated by scaling parameters estimated for mice. The good agreement between simulated and observed bortezomib concentrations after multiple dosing [27] demonstrated the qualitative and quantitative similarity of target-mediated bortezomib disposition in mice and humans (Fig. 5a). Furthermore, the final model was used to predict bortezomib plasma PK

profiles in humans for varying glomerular filtration rate (GFR) values after multiple dosing treatment, and the simulations suggest that renal impairment exerts a minimal influence on bortezomib exposure in humans (Fig. 5b).

DISCUSSION

Despite its extensive and successful clinical use, bortezomib PK is not fully characterized in preclinical species or humans. Several bortezomib PK studies have been performed in rats and mice [8, 28]; however, none of these studies were able to capture the long terminal elimination phase or provide a suitable dose-ranging study for exploring the mechanism of bortezomib nonlinear disposition. Using a validated and sensitive LC/MS/MS assay, this current study enabled the resolution of the long terminal phase at multiple dosing levels in various tissues over six days. With this extensive PK data, a PBPK model was successfully developed for investigating the influence of saturable drug-target binding on bortezomib tissue distribution in mice. In addition, the scaled PBPK model recapitulated human plasma PK profiles following multiple dosing and can serve as a physiological platform for predicting bortezomib concentrations in inaccessible target tissues for clinical dosing regimen optimization.

Initially, we attempted to apply a published PBPK model for everolimus, which incorporates nonlinear drug-tissue binding [29]. The model assumes that blood and tissue are “well-stirred” compartments and that unbound drug is in instantaneous equilibrium between tissue and capillary blood [29]. However, the prolonged bortezomib half-life in non-eliminating tissues, such as the spleen and bone, necessitated the inclusion of a permeability-limited distribution term to capture the prolonged terminal phase of these tissues, particularly at the lower dose. Initially, renal clearance was proposed to be nonlinear, but such a structure resulted in imprecise parameter estimates. Instead, attempts of fixing renal clearance at *GFR* values successfully captured bortezomib PK profiles with reasonable parameter estimates. Liver concentrations at the higher dose level (1 mg/kg) were overestimated (Figure 3). To improve model performance, a series of models with nonlinear functions were attempted but resulted in unidentifiable parameter estimates. It is not clear whether transporters or other distribution processes might be responsible for the model misspecification. Bortezomib exhibits linear hepatic metabolism at clinically relevant concentrations [6], and given the good model fitting for all other profiles, the linear hepatic clearance was retained in the final model. Early attempts at estimating the vascular fraction of the remainder compartment ($fv_{,re}$) also resulted in unidentifiable estimates. Considering that adipose tissue constitutes approximately 40% of the mass of the remainder space [23], fixing the $fv_{,re}$ term to literature reported adipose vascular fraction [24] greatly improved the PBPK model performance. In addition, the permeability-based model structure provided a basis for separating tissues into three subcompartments, namely tissue plasma, RBC, and extravascular spaces, which facilitated an assessment of the influence of drug-target binding in capillary RBC on bortezomib tissue uptake when blood transits through tissues. The final PBPK model also provides a physiological platform for evaluating the influence of system- specific (e.g., target density) and drug-specific (e.g., K_D) perturbations on bortezomib tissue selectivity. A model sensitivity analysis indicates that bortezomib concentrations in tissue are relatively

insensitive to changes in K_D as compared to the significant tissue partitioning elicited by changes in target density (Supplementary Fig. S2).

Proteasome is a highly conserved protease complex in the cytoplasm and expressed in all tissues with varying densities. Bortezomib exhibits reversible high affinity binding to proteasome with slow dissociation kinetics [2]. The distribution of proteasome in tissue significantly influences bortezomib tissue selectivity as well as efficacy profiles. The final PBPK model, which was developed with regional proteasome/bortezomib binding kinetics, affords a mechanism-based platform for assessing drug-target binding kinetics on bortezomib tissue selectivity. Of all the tested tissues, erythrocytes possess the greatest target density, which is consistent with literature measurements in rats [2]. Owing to the high abundance of proteasome in erythrocytes and slow dissociation kinetics, a substantial fraction of bortezomib molecules are expected to rapidly bind but slowly dissociate from proteasome in erythrocytes, and thus might limit distribution outside of the blood compartment to tissues with lower proteasome density, such as muscle and bone. Bortezomib shows synergistic effects when combined with an irreversible proteasome inhibitor, which might be attributed to the apparent change in blood and tumor target capacity when these agents compete for the target binding sites in blood, consequently altering bortezomib tissue distribution profiles in tumor [2, 30, 31].

Conventional allometric scaling seeks to empirically establish a power-law relationship between PK parameters among different species and bodyweight. Without considering the potential dose-dependence in drug distribution and elimination, classic allometry can be problematic in scaling drugs with TMDD properties [32]. In contrast, our PBPK model was developed based on system-specific properties (e.g., target density) and drug-specific properties (e.g., K_D), yielding a mechanistic approach for predicting bortezomib PK in humans by appropriately scaling or calculating multiple factors independently. During the scaling process, tissue target densities and bortezomib binding affinity in humans were assumed to be identical with those in mice. In addition, human tissue permeability and hepatic intrinsic clearance were scaled against bodyweight using theoretically expected allometric exponents. The scaled human PBPK model successfully recapitulated bortezomib plasma PK profiles after multiple dosing and supports the hypothesis of target-mediated bortezomib disposition in humans. Bortezomib is partially eliminated by renal excretion in humans, and renal impairment is a frequent complication in MM, with more than 50% of patients developing some form of renal dysfunction during the course of disease. The scaled human PBPK model predicts that renal clearance contributes to 26% of overall bortezomib elimination in human, which is comparable to the measured renal clearance contribution (approximately 25%) in monkeys [33]. In addition, the final model predicts that renal impairment should have minimal influence on bortezomib exposure in humans. This simulation is consistent with clinical observations from patients with renal impairment [34], confirming that bortezomib dose-adjustment is not necessary for MM patients with renal dysfunction.

In keeping with basic principles of TMDD, bortezomib plasma PK appears time-dependent in humans, in which the terminal half-life in plasma prolongs in the first dosing cycle and then stabilizes in subsequent cycles [27]. Apart from linear metabolism kinetics, bortezomib

is not an inducer or inhibitor of enzymes responsible for its elimination; therefore, the apparent time-dependent disposition of bortezomib might manifest from its nonlinear target-binding [35]. In addition, humans receive lower bortezomib doses than were tested in mice (per kg body weight), resulting in relative lower ranges of plasma and tissue concentrations. Owing to the high capacity of proteasome in tissues, TMDD theory suggests that the volume of distribution of bortezomib might steadily increase under such conditions prior to the steady increase of tissue target binding (i.e., before tissue proteasome is fully occupied) during multiple dosing schemes. Accordingly, proteasome-mediated bortezomib distribution was attributed to its concentration- and time-dependent kinetics following multiple dosing in human.

Drug plasma concentrations are commonly used to drive PD effects; however, the use of plasma concentration is questionable for accurately predicting bortezomib clinical efficacy. This is underscored by the fact that bortezomib PK differs markedly between plasma and target tissues (e.g., bone) due to extensive tissue drug-target binding. Therefore, characterizing bortezomib concentrations at target sites is critical for clinical dosing regimen optimization. The final scaled PBPK model in this study may serve as a platform for predicting bortezomib concentrations in inaccessible target and toxicity-related tissues in humans, which can be further linked to downstream PD biomarkers for a mechanism-based exposure-efficacy study to maximize bortezomib therapeutic efficacy as well as minimize adverse effects.

CONCLUSION

In this study, a bortezomib PBPK model incorporating tissue drug-target binding was developed in mice. The PBPK model reasonably captures bortezomib concentrations in plasma and various tissues at multiple dosing levels. The PBPK model was further scaled to humans and successfully recapitulated bortezomib plasma PK profiles after multiple dosing in humans. This further supports the hypothesis that proteasome-mediated bortezomib disposition is the primary source of its dose- and time-dependent kinetics. Model simulations show that renal impairment has minimal impact on bortezomib exposure in humans, confirming that bortezomib dose adjustment is not necessary for MM patients with renal impairment.

Supplementary Material

Refer to Web version on PubMed Central for supplementary material.

Acknowledgments

This work was supported by National Institutes of Health [Grant GM57980]. The authors declare no conflicts of interest that would influence this work. We thank Ms. Donna Ruszaj for her valuable technique assistance in developing the LC/MS/MS assay.

References

1. Richardson PG, Mitsiades C, Hideshima T, Anderson KC. Bortezomib: proteasome inhibition as an effective anticancer therapy. Annu Rev Med. 2006; 57:33–47. [PubMed: 16409135]

2. Dick LR, Fleming PE. Building on bortezomib: second-generation proteasome inhibitors as anti-cancer therapy. Drug Discov Today. 2010; 15:243–249. [PubMed: 20116451]
3. Lieu C, Chow L, Pierson AS, Eckhardt SG, O'Bryant CL, Morrow M, Tran ZV, Wright JJ, Gore L. A phase I study of bortezomib, etoposide and carboplatin in patients with advanced solid tumors refractory to standard therapy. Invest New Drugs. 2009; 27:53–62. [PubMed: 18618082]
4. Mateos MV. How to maintain patients on long-term therapy: understanding the profile and kinetics of adverse events. Leuk Res. 2012; 36(Suppl 1):S35–43. [PubMed: 23176723]
5. Bross PF, Kane R, Farrell AT, Abraham S, Benson K, Brower ME, Bradley S, Gobburu JV, Goheer A, Lee SL, Leighton J, Liang CY, Lostritto RT, McGuinn WD, Morse DE, Rahman A, Rosario LA, Verbois SL, Williams G, Wang YC, Pazdur R. Approval summary for bortezomib for injection in the treatment of multiple myeloma. Clin Cancer Res. 2004; 10:3954–3964. [PubMed: 15217925]
6. Uttamsingh V, Lu C, Miwa G, Gan LS. Relative contributions of the five major human cytochromes P450, 1A2, 2C9, 2C19, 2D6, and 3A4, to the hepatic metabolism of the proteasome inhibitor bortezomib. Drug Metab Dispos. 2005; 33:1723–1728. [PubMed: 16103134]
7. Leveque D, Carvalho MC, Maloisel F. Review. Clinical pharmacokinetics of bortezomib. In Vivo. 2007; 21:273–278. [PubMed: 17436576]
8. Hemeryck A, Geerts R, Monbaliu J, Hassler S, Verhaeghe T, Diels L, Verluyten W, van Beijsterveldt L, Mamidi RN, Janssen C, De Coster R. Tissue distribution and depletion kinetics of bortezomib and bortezomib-related radioactivity in male rats after single and repeated intravenous injection of 14 C-bortezomib. Cancer Chemother Pharmacol. 2007; 60:777–787. [PubMed: 17285316]
9. Akhlaghi, F.; Monbaliu, J.; Kadambi, V.; Li, Y. [Accessed 9 Oct 2009] Blood and Plasma Pharmacokinetics of Bortezomib in Relation to Blood 20S Proteasome Activity after Single and Multiple Dosing in Cynomongolus Monkeys. 2009. http://www2009go-acoporg/acop2009
10. McConkey DJ, Zhu K. Mechanisms of proteasome inhibitor action and resistance in cancer. Drug Resist Updat. 2008; 11:164–179. [PubMed: 18818117]
11. Tanaka K, Ii K, Ichihara A, Waxman L, Goldberg AL. A high molecular weight protease in the cytosol of rat liver. I. Purification, enzymological properties, and tissue distribution. J Biol Chem. 1986; 261:15197–15203. [PubMed: 3095325]
12. Levy G. Pharmacologic target-mediated drug disposition. Clin Pharmacol Ther. 1994; 56:248–252. [PubMed: 7924119]
13. Mager DE. Target-mediated drug disposition and dynamics. Biochem Pharmacol. 2006; 72:1–10. [PubMed: 16469301]
14. Diao L, Meibohm B. Pharmacokinetics and pharmacokinetic-pharmacodynamic correlations of therapeutic peptides. Clin Pharmacokinet. 2013; 52:855–868. [PubMed: 23719681]
15. Singh J, Petter RC, Baillie TA, Whitty A. The resurgence of covalent drugs. Nat Rev Drug Discov. 2011; 10:307–317. [PubMed: 21455239]
16. Mager DE, Jusko WJ. General pharmacokinetic model for drugs exhibiting target-mediated drug disposition. Journal of pharmacokinetics and pharmacodynamics. 2001; 28:507–532. [PubMed: 11999290]
17. Gibiansky L, Gibiansky E, Kakkar T, Ma P. Approximations of the target-mediated drug disposition model and identifiability of model parameters. Journal of pharmacokinetics and pharmacodynamics. 2008; 35:573–591. [PubMed: 19005743]
18. Dua P, Hawkins E, Van der Graaf P. A tutorial on target-mediated drug disposition (TMDD) models. CPT: pharmacometrics & systems pharmacology. 2015; 4:324–337. [PubMed: 26225261]
19. Rowland M, Peck C, Tucker G. Physiologically-based pharmacokinetics in drug development and regulatory science. Annu Rev Pharmacol Toxicol. 2011; 51:45–73. [PubMed: 20854171]
20. Levy G, Mager DE, Cheung WK, Jusko WJ. Comparative pharmacokinetics of coumarin anticoagulants L: Physiologic modeling of S-warfarin in rats and pharmacologic target-mediated warfarin disposition in man. J Pharm Sci. 2003; 92:985–994. [PubMed: 12712418]
21. Davies B, Morris T. Physiological parameters in laboratory animals and humans. Pharm Res. 1993; 10:1093–1095. [PubMed: 8378254]

22. Adams J, Palombella VJ, Sausville EA, Johnson J, Destree A, Lazarus DD, Maas J, Pien CS, Prakash S, Elliott PJ. Proteasome inhibitors: a novel class of potent and effective antitumor agents. Cancer Res. 1999; 59:2615–2622. [PubMed: 10363983]

23. Brown RP, Delp MD, Lindstedt SL, Rhomberg LR, Beliles RP. Physiological parameter values for physiologically based pharmacokinetic models. Toxicol Ind Health. 1997; 13:407–484. [PubMed: 9249929]

24. Kawai R, Mathew D, Tanaka C, Rowland M. Physiologically based pharmacokinetics of cyclosporine A: extension to tissue distribution kinetics in rats and scale-up to human. J Pharmacol Exp Ther. 1998; 287:457–468. [PubMed: 9808668]

25. D'Argenio, DZ.; Schumitzky, A.; Wang, X. ADAPT 5 user's guide: pharmacokinetic/ pharmacodynamic systems analysis software. Biomedical Simulation Resource; Los Angeles, CA: 2009.

26. Tsu C, Blank J, Garcia K, Liu J, Bruzzese F, Lee E, Cao Y, Bannerman B, Fitzgerald M, Fleming P, Ciavarri J, Hales P, Yu J, Yang Y, Berger A, Sintchak M, Kupperman E, Manfredi M, Dick L. Beyond Bortezomib: Development of Millennium's Next-Generation Proteasome Inhibitors. Mol Cancer Ther. 2011; 2011 doi:101158/1535-7163TARG-11-C99.

27. Reece DE, Sullivan D, Lonial S, Mohrbacher AF, Chatta G, Shustik C, Burris H 3rd, Venkatakrishnan K, Neuwirth R, Riordan WJ, Karol M, von Moltke LL, Acharya M, Zannikos P, Keith Stewart A. Pharmacokinetic and pharmacodynamic study of two doses of bortezomib in patients with relapsed multiple myeloma. Cancer Chemother Pharmacol. 2011; 67:57–67. [PubMed: 20306195]

28. Kupperman E, Lee EC, Cao Y, Bannerman B, Fitzgerald M, Berger A, Yu J, Yang Y, Hales P, Bruzzese F, Liu J, Blank J, Garcia K, Tsu C, Dick L, Fleming P, Yu L, Manfredi M, Rolfe M, Bolen J. Evaluation of the proteasome inhibitor MLN9708 in preclinical models of human cancer. Cancer Res. 2010; 70:1970–1980. [PubMed: 20160034]

29. Laplanche R, Meno-Tetang GM, Kawai R. Physiologically based pharmacokinetic (PBPK) modeling of everolimus (RAD001) in rats involving non-linear tissue uptake. J Pharmacokinet Pharmacodyn. 2007; 34:373–400. [PubMed: 17431753]

30. Chauhan D, Singh A, Brahmandam M, Podar K, Hideshima T, Richardson P, Munshi N, Palladino MA, Anderson KC. Combination of proteasome inhibitors bortezomib and NPI-0052 trigger in vivo synergistic cytotoxicity in multiple myeloma. Blood. 2008; 111:1654–1664. [PubMed: 18006697]

31. Williamson MJ, Blank JL, Bruzzese FJ, Cao Y, Daniels JS, Dick LR, Labutti J, Mazzola AM, Patil AD, Reimer CL, Solomon MS, Stirling M, Tian Y, Tsu CA, Weatherhead GS, Zhang JX, Rolfe M. Comparison of biochemical and biological effects of ML858 (salinosporamide A) and bortezomib. Mol Cancer Ther. 2006; 5:3052–3061. [PubMed: 17172407]

32. Kagan L, Abraham AK, Harrold JM, Mager DE. Interspecies scaling of receptor-mediated pharmacokinetics and pharmacodynamics of type I interferons. Pharmaceutical research. 2010; 27:920–932. [PubMed: 20232116]

33. Nix D, Press R, Wehrman T, Aide R. Tissue Distribution and Mass Balance of Bortezomib (Velcade™) in Non-Human Primates. AAPS PharmSci. 2003; 5:4.

34. Leal TB, Remick SC, Takimoto CH, Ramanathan RK, Davies A, Egorin MJ, Hamilton A, LoRusso PA, Shibata S, Lenz HJ, Mier J, Sarantopoulos J, Mani S, Wright JJ, Ivy SP, Neuwirth R, von Moltke L, Venkatakrishnan K, Mulkerin D. Dose-escalating and pharmacological study of bortezomib in adult cancer patients with impaired renal function: a National Cancer Institute Organ Dysfunction Working Group Study. Cancer chemotherapy and pharmacology. 2011; 68:1439–1447. [PubMed: 21479634]

35. Lu C, Gallegos R, Li P, Xia CQ, Pusalkar S, Uttamsingh V, Nix D, Miwa GT, Gan LS. Investigation of drug-drug interaction potential of bortezomib in vivo in female Sprague-Dawley rats and in vitro in human liver microsomes. Drug Metab Dispos. 2006; 34:702–708. [PubMed: 16443666]

36. Levy G. Kinetics of pharmacologic effects. Clinical pharmacology and therapeutics. 1966; 7:362–372. [PubMed: 5937003]

37. Lappin G, Kuhnz W, Jochemsen R, Kneer J, Chaudhary A, Oosterhuis B, Drijfhout WJ, Rowland M, Garner RC. Use of microdosing to predict pharmacokinetics at the therapeutic dose: experience with 5 drugs. Clinical pharmacology and therapeutics. 2006; 80:203–215. [PubMed: 16952487]

Postscript

DEM was first introduced to the basic concepts of the kinetics of pharmacologic effects as an undergraduate pharmacy student at The University at Buffalo, SUNY by Dr. Gerhard Levy (GL). Although GL's landmark paper was published over two decades prior [36], few schools of pharmacy were providing undergraduates with training in the emerging field of pharmacodynamics. In contrast, GL shared his groundbreaking discoveries with pharmacy students and provided them with unique undergraduate research opportunities. Years later, DEM was invited to join the laboratory of Dr. William J. Jusko (WJJ), a former graduate of GL's laboratory and world-renowned expert in PK/PD. In the course of DEM's graduate research, consideration of the complex disposition properties of therapeutic proteins led to the hypothesis that nonlinear distribution and elimination processes, although well-described with separate Michaelis-Menten functions, could both manifest and be characterized by a general binding model [16] based on the principles of TMDD identified by GL [12]. Following this publication, GL returned to Buffalo with slides, data, and a collaborative research proposal, which resulted in the PBPK model of warfarin TMDD [20]. The work progressed rapidly owing to GL's uncanny ability to ask questions that went to the very heart of the matter and to be ever ready with the next set of *in silico* experiments upon reaching each milestone. Interestingly, predictions by the model that warfarin should exhibit very rapid distribution and a relatively long terminal half-life at very low doses were ultimately confirmed by a microdosing clinical study [37]. Warfarin and bortezomib share similarities in that both are classified as covalent inhibitors and target ubiquitously expressed enzymes [15]. DEM and LZ are indebted to the vision and pioneering research of GL on TMDD and pharmacodynamics. His early and deep insights into the clinical and developmental implications of TMDD have served as inspiration for decades of PK/PD model development for understanding the concentration-effect relationships of many complex compounds now and for likely years to come.

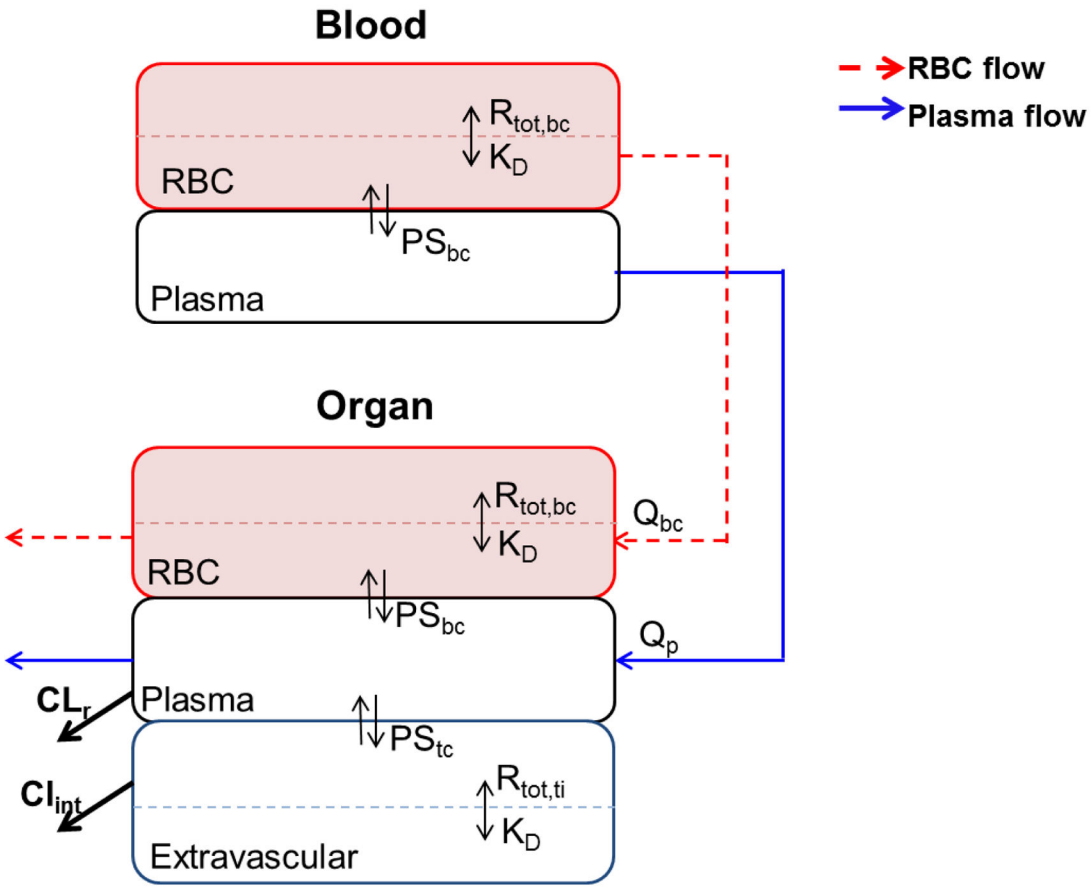

Fig. 1.

Schematic of a local bortezomib PK model in mice. Blood is subdivided into RBC and plasma spaces. Each tissue is divided into vascular and extravascular subcompartments, wherein, tissue vasculature is further subdivided into tissue RBC and plasma spaces. The nonlinear drug-target binding occurs in RBC, tissue RBC, and extravascular subcompartments with the same target binding affinity K_D. Bortezomib is eliminated from the kidney plasma space with renal clearance of CL_r, and from liver extravascular space with hepatic clearance of CL_{int}.

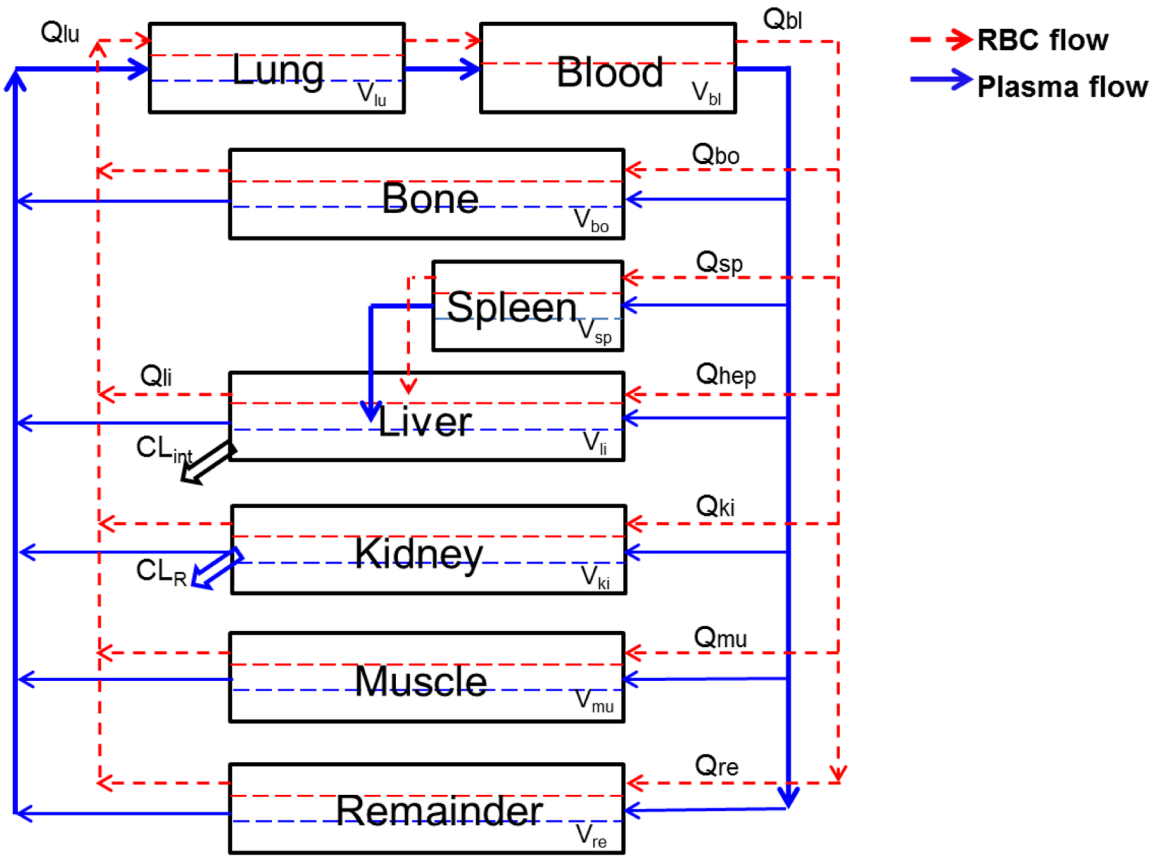

Fig. 2.

Schematic of a full bortezomib global PBPK model in mice. Blood and tissues are connected in an anatomical manner by plasma flow (solid line) and RBC flow (dashed line). Detailed description of bortezomib disposition in each tissue is shown in Fig. 1. The clearance is denoted by a renal clearance from kidney plasma space and a hepatic clearance from the liver extravascular subcompartment. The physiological values of tissue blood flow (Q_{ti}) and and volume (V_{ti}) for each tissue are reported in Table 2.

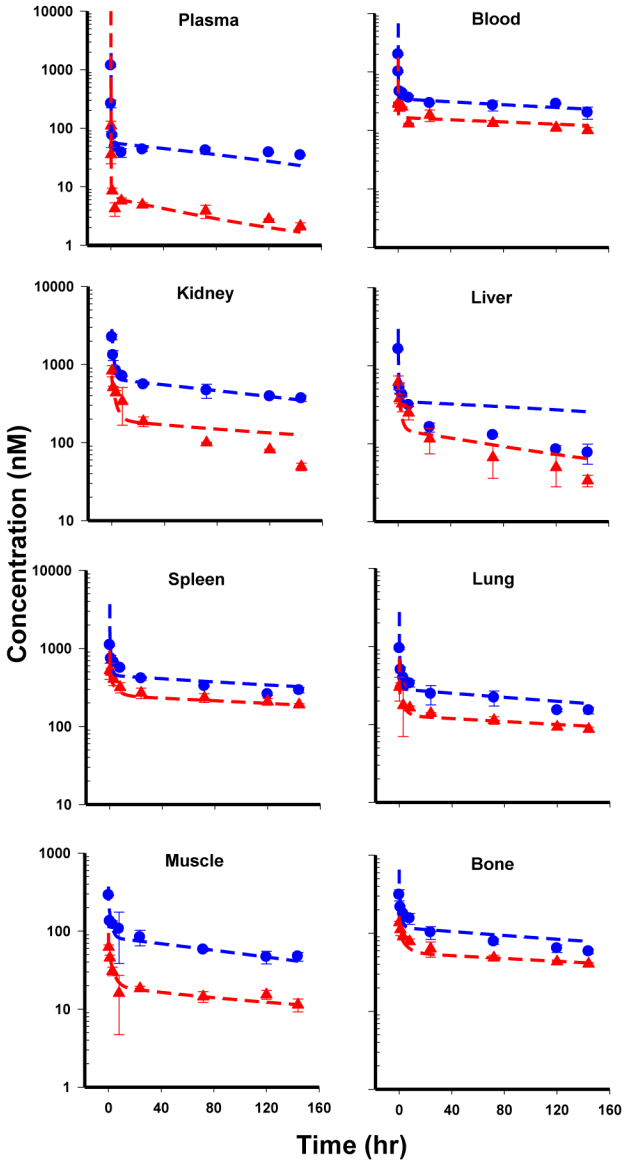

Fig. 3.

Time-course of bortezomib concentrations in plasma and tissues of mice following single IV dosing at 0.25 and 1 mg/kg. The red triangles are measured bortezomib concentrations (mean ± SD, n=3) in plasma and tissue following 0.25 mg/kg dosing. The blue circles represent measured bortezomib concentrations (mean ± SD, n=3) in plasma and tissue following 1 mg/kg dosing. Dashed lines represent PBPK modeling fitted profiles.

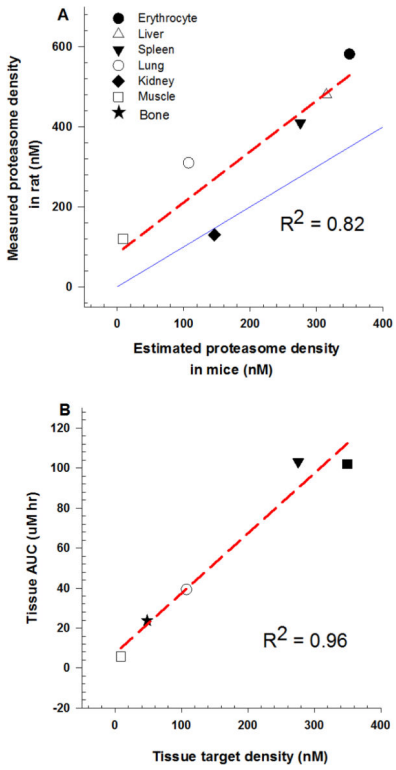

Fig. 4.

(a) Rank-order correlation of model estimated proteasome density in mice versus experimentally reported proteasome concentrations in rats obtained from the literature [9, 11]. Symbols on x-axis are PBPK model estimated tissue target densities in mice. Symbols on y axis are experimentally reported tissue proteasome concentrations in rats. The red dashed line is a regression line, and the blue solid line represents the line of identity. (b) Rank-order correlation of model estimated proteasome density in mice versus bortezomib tissue AUC values at 0.25 mg/kg. Symbols on x-axis are PBPK model estimated tissue target densities in mice. Symbols on y-axis represent bortezomib tissue AUC value at 0.25 mg/kg. Red dashed line represents regression line.

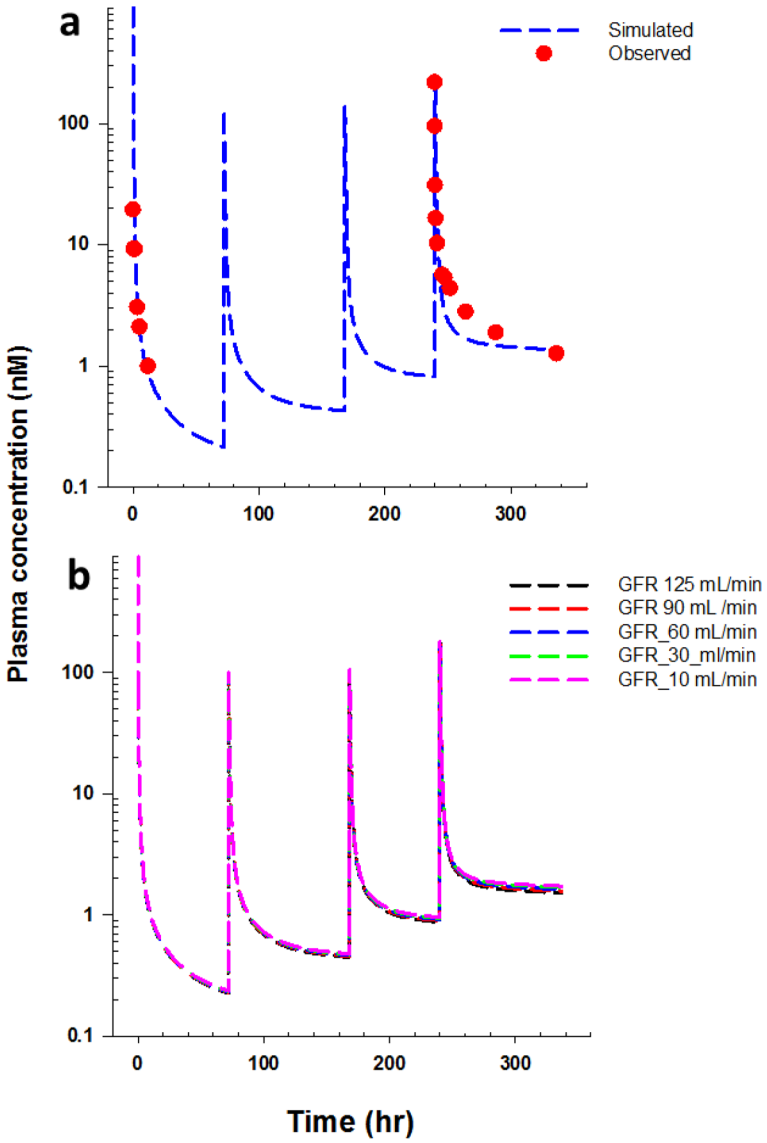

Fig. 5.

(a) Time-course of bortezomib plasma concentrations in humans following 1.3 mg/m^2 bortezomib IV administration on day 1, 4, 8, and 11. Solid circles represent mean data extracted from reference [27], and dashed lines are PBPK model predicted profiles based on an interspecies scaling approach. (b) Model simulated bortezomib plasma concentration following 1.3 mg/m^2 bortezomib IV administration on day 1, 4, 8 and 11 under different glomerular filtration rates (GFR) in humans. Dashed lines are PBPK model predicted bortezomib human plasma PK profiles under varying GFR values.

Table 1

Bortezomib Plasma and Tissue PK Non-Compartmental Analysis

Tissue	$AUC_{0\text{-}inf}$ (μM·hr)		K_p		Half-life (hr)	
	0.25 mg/kg	1 mg/kg	0.25 mg/kg	1 mg/kg	0.25 mg/kg	1 mg/kg
Plasma	0.9	19.4	1.0	1.0	96	267
Blood	46.4	92.0	52.8	4.8	182	173
Muscle	5.7	17.3	6.4	0.9	204	112
Kidney	24.7	179.6	N/A	N/A	59	204
Spleen	103.1	106.9	117.3	5.5	248	131
Liver	17.0	33.3	N/A	N/A	69	105
Lung	39.3	60.9	44.7	3.1	178	133
Bone	23.7	27.2	26.9	1.4	277	173

$AUC_{0\text{-}inf}$ represents area under plasma or tissue concentration-time curve from time 0 to infinity, K_p is the ratio of tissue-to-plasma $AUC_{0\text{-}inf}$. N/A, not applicable.

J Pharmacokinet Pharmacodyn. Author manuscript; available in PMC 2016 October 01.

Table 2

Physiological Parameters for Bortezomib PBPK Modeling

Tissue	Blood flow (Q_{ti})		Tissue volume (V_{ti})		Vascular fraction ($fv_{,ti}$)
	Mice (mL/min)	Human (L/hr)	Mice (mL)	Human (L)	
Blood	13.98	312	1.23	5.2	--
Lung	13.98	312	0.18	1.17	0.262
Spleen	0.15	4.62	0.09	0.19	0.282
Liver	2.25	70.82	1.37	1.69	0.115
Kidney	1.27	54.60	0.42	0.28	0.105
Muscle	2.23	59.59	9.60	28.00	0.026
Bone	0.46	13.10	2.68	10.01	0.041
Remainder	7.77	113.88	9.44	23.46	0.010[a]

Data are extracted from Ref [21, 23, 24]

[a]Value is fixed to adipose vascular fraction

J Pharmacokinet Pharmacodyn. Author manuscript; available in PMC 2016 October 01.

Table 3

Estimated PK Parameters of Bortezomib in Mice using a Global PBPK Model

Tissue	Permeability ($PS_{tc,ti}$)		Target density (R_{ti})		Nonspecific binding (NS_{ti})		Clearance	
	mL/min	CV%	nM	CV%	--	CV%	mL/min	CV%
Erythrocyte	17.0	--[a]	349.8	10.69	7.57	15.21	--[c]	--[c]
Lung	0.013	30.71	107.4	19.65	2.54	31.32	--[c]	--[c]
Spleen	0.01	27.91	275.7	15.11	3.68	35.84	--[c]	--[c]
Liver	0.287	23.12	315.0	19.27	1.54	45.02	0.0063	17.49
Kidney	0.069	22.88	146.2	17.56	9.60	17.95	0.28	--[b]
Muscle	0.123	22.42	8.60	27.83	1.17	17.57	--[c]	--[c]
Bone	0.072	24.40	48.12	15.03	1.06	27.40	--[c]	--[c]
Remainder	4.17	12.47	970	14.09	96.76	11.75	--[c]	--[c]

[a] Fixed to estimate from individual tissue fitting stage

[b] Fixed to reported GFR value in mice from Ref [21]

[c] Not used in the model

J Pharmacokinet Pharmacodyn. Author manuscript; available in PMC 2016 October 01.